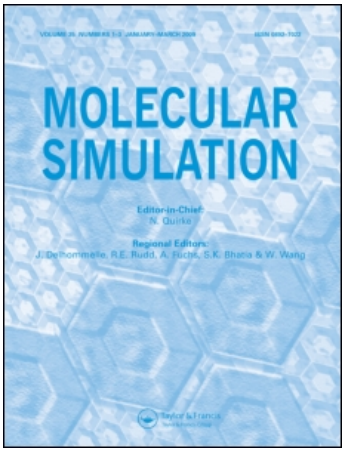

Molecular Simulation
Publication details, including instructions for authors and subscription information:
http://www.informaworld.com/smpp/title~content=t713644482

Faceted nanoparticles in a nematic liquid crystal: defect structures and potentials of mean force

Francisco R. Hung[a]; Shivkumar Bale[a]
[a] Cain Department of Chemical Engineering, Louisiana State University, Baton Rouge, LA, USA

To cite this Article Hung, Francisco R. and Bale, Shivkumar(2009) 'Faceted nanoparticles in a nematic liquid crystal: defect structures and potentials of mean force', Molecular Simulation, 35: 10, 822 — 834
To link to this Article: DOI: 10.1080/08927020902801563
URL: http://dx.doi.org/10.1080/08927020902801563

Molecular Simulation
Vol. 35, Nos. 10–11, September 2009, 822–834

Taylor & Francis
Taylor & Francis Group

Faceted nanoparticles in a nematic liquid crystal: defect structures and potentials of mean force

Francisco R. Hung* and Shivkumar Bale

Cain Department of Chemical Engineering, Louisiana State University, Baton Rouge, LA 70803, USA

(*Received 23 December 2008; final version received 30 January 2009*)

We investigate the defect structures and the potentials of mean force (PMF) that arise when faceted nanoparticles, namely cubes and triangular prisms, are immersed in a nematic liquid crystal (NLC). Using a mesoscale theory for the tensor order parameter **Q** of the nematic, we have determined the thermodynamic stability of different orientations of one nanoparticle with respect to the far-field director **n**(**r**). A nanocube with perpendicular anchoring of the nematic at its surfaces tends to align in such a way that none of its faces is parallel or perpendicular to **n**(**r**); the most stable defect structure consists of a distorted Saturn ring with sharp bends, which covers six of the edges of the cubic particle. In contrast, a triangular nanoprism with homeotropic anchoring of the nematic at its surfaces tends to align with its long axis perpendicular to the far-field director **n**(**r**), and with one of its rectangular faces perpendicular to **n**(**r**). For such a configuration, the defect structure consists of two large disclination regions covering the two triangular faces of the prism, and two narrow disclination regions surrounding two of the rounded edges of the prism. We also studied the thermodynamic stability of different arrays of two particles, finding that for two nanocubes that approach each other keeping their orientations fixed, the nematic forms a distorted 'entangled hyperbolic' defect structure around the particles, in analogy to what was observed for pairs of spherical and spherocylindrical nanoparticles in close proximity. The NLC-mediated interactions between the nanocubes in this case are of the order of $-85k_BT$, which are weaker than those observed for spherical nanoparticles of comparable diameter ($\sim -110k_BT$). For systems of two nanoprisms having their long axes perpendicular to the far-field director, we considered three particle arrays: linear (the long axes of the particles are collinear and the particles have the same orientation), parallel (the long axes of the particles are parallel and the particles have the same orientation) and inverted parallel (the long axes of the particles are parallel, and one of the prisms is inverted with respect to the other one). Our results suggest that inverted parallel arrays are thermodynamically more stable than linear arrays, which in turn are more stable than parallel arrays. The minima observed in the PMF curves for the inverted parallel ($\sim -1050k_BT$) and linear arrays ($\sim -525k_BT$) are significantly deeper than that observed for the parallel array ($\sim -150k_BT$). In comparison, a pair of nanospheres with a diameter comparable to the size of the triangular faces of our nanoprisms has a PMF minimum of $\sim 73k_BT$ when the spheres are in close proximity. These NLC-mediated, anisotropic interparticle interactions can make the particles bind together at specific locations, and thus could be used to assemble the particles into ordered structures with different morphologies.

Keywords: nanocubes; nanoprisms; nematic liquid crystal; mesoscale theory; simulation

1. Introduction

Systems of particles dispersed in liquid crystals (LCs) have recently attracted attention for the development of novel materials. The inclusion of the particles in the LC produces a distortion in its director field. As a result, the LC and the particles will rearrange as to minimise the elastic perturbations, giving rise to long-range interparticle interactions that can induce the formation of a number of ordered colloid structures [1–6]. The LC-mediated interparticle interactions are anisotropic and can reach up to several thousands of k_BT, according to recent experiments [1,3,4,6,7] and calculations [4,6,8–10]. These LC-mediated interactions depend on the size and shape of the particles, the local anchoring of the LC at the particles' surfaces, the alignment of the director field far away from the particles, and the geometry of the surroundings (i.e. presence of walls, channels and other confining elements). Although most of the experimental work mentioned above has focused on systems of spherical, micron-sized colloids in LCs, a number of experimental studies [11] have considered systems of nanoparticles in LCs. LCs have been used to manipulate and organise spherical [12–16], as well as rod-like nanoparticles such as nickel nanowires and carbon nanotubes [17–20]. These systems have potential applications in light-scattering devices, electro-optical switches, photonics, nanoscale electronics and LC displays. Systems of nanoparticles in LCs are also relevant for the development of optical sensors. Recent experiments [21–24] and calculations [25–27] have demonstrated that the binding of chemicals, biomolecules and viruses at solid-LC and liquid-LC functionalised interfaces perturbs the local ordering of the LC, and triggers the formation of inhomogeneous textures. These inhomogeneities can then be amplified by the LC over several length scales, and thus be detected using polarised optical microscopy.

*Corresponding author. Email: frhung@lsu.edu

ISSN 0892-7022 print/ISSN 1029-0435 online

DOI: 10.1080/08927020902801563
http://www.informaworld.com

The behaviour of a dispersion of particles in LCs is dictated by the formation of defects by the LC around the particles. The uniform alignment of an LC is distorted by the inclusion of particles, due to the constraints imposed by the anchoring of the LC at the surfaces of the particles. These constraints impose conflicting orientations to the LC, resulting in the formation of topological defects. These defects are characterised by discontinuities in the director field $\mathbf{n}(\mathbf{r})$ and a pronounced decrease in the scalar order parameter $S(\mathbf{r})$, reflecting the fact that the LC melts at the core of the defects [28]. For the simplest case of a single spherical particle in a nematic LC, three types of defects have been observed experimentally: the dipole configuration (where the nematic forms a point defect known as hyperbolic hedgehog) [1,29]; the Saturn ring configuration (where the particle is surrounded by a disclination loop) [29–31]; and the surface ring configuration (where the nematic forms a disclination ring sitting at the surface of the particle) [1,29]. These defect structures have been the focus of several theoretical and computational studies [29,32–38]. The dipole configuration is stable for strong surface anchoring and micron-sized spherical particles. The Saturn ring configuration was predicted to become stable upon reduction of particle size, which was confirmed experimentally very recently [39]. Magnetic and electric fields [40], and confinement conditions [31,36,41] were also found to stabilise a Saturn ring configuration. A surface ring defect is observed upon reduction of the surface anchoring strength [29,34]. Systems involving two spherical particles exhibiting dipole [42] and Saturn ring [8] configurations have been recently examined using a mesoscale theory where the nematic is described using the tensor order parameter $\mathbf{Q}(\mathbf{r})$. The predictions of the mesoscale theory were satisfactorily compared with those from molecular simulations [8], providing a measure of the validity of the theory at nm-length scales. As a result, the mesoscale theory, which is computationally less expensive than molecular simulations, was used to study the stability of arrays of several spherical nanoparticles in a nematic in the bulk [8] and inside nanochannels [10], as well as the stability of arrays of spherocylindrical nanoparticles in a nematic [9]. Classical density functional theory has been used recently to study the structure of an LC around a cylindrical particle of infinite length, to calculate the forces between two of these particles, and to study the interactions of such particles with structured substrates [43]. Very recently, several groups have performed dynamical simulations in 2D and 3D systems, where disks or spherical particles are free to move due to the many-body forces mediated by the LC [44–47]. Very recently, Hung [48] investigated the effects of particle shape and size on the defect structures and the interparticle interactions in systems of nm- and μm-sized spherical and spherocylindrical particles immersed in a nematic.

Most of the studies mentioned above have concentrated on spherical and spherocylindrical particles immersed in a nematic LC. Novel chemical, physical and biological-inspired methods have resulted in the synthesis of particles with unique shapes and anisotropic interactions [49,50], which can exhibit unique physical and chemical properties. These anisotropic particles can also be used as building blocks in the development of ordered structures with unique properties. In particular, LC-mediated interactions can be used to assemble and hold the anisotropic particles together in organised structures. Due to the large variety of particle shapes and anisotropies available, computer simulations are well suited to systematically explore and quickly predict the behaviour of systems of non-spherical particles in LCs. These studies could influence and possibly even guide future experimental efforts in the area.

The objective of this paper is to determine the nature of the defect structures formed around nm-sized faceted particles, namely cubic particles [51,52] and triangular prisms [53,54]. In all cases, the stability of the systems will be determined by calculating their free energies. The formation of defect structures around groups of particles in a nematic is important since strong, anisotropic interparticle interactions usually develop. Furthermore, the strength and degree of anisotropy in the interparticle interactions is expected to vary when particles of shape other than spherical are considered. These interparticle interactions can thus be used to assemble and hold together non-spherical particles into ordered arrays with morphologies different from the hexagonal, close-packed structures formed by spherical particles. Such a subject has attracted a great deal of attention recently [49,55]. The paper is organised as follows. In Section 2 we present a description of our model systems and details of the computational methodology. Section 3 contains our results and discussion, and our concluding remarks are presented in Section 4.

2. Models and methods

2.1 Details of the model systems

The model system considered in this work consists of a rectangular box (nematic cell) of dimensions L_x, L_y and L_z, containing one or two particles immersed in a nematic LC. A schematic of the nematic cell containing one cubic nanoparticle is shown in Figure 1(a). We have imposed periodic boundary conditions in the x and y directions of the nematic cell, and we have placed walls at the top and bottom faces of the nematic cell, which impose homeotropic anchoring to the nematic. Homeotropic anchoring is also imposed to the nematic at the surfaces of the particles. Such conditions can be easily achieved experimentally, e.g. by coating the surfaces with self-assembled monolayers of

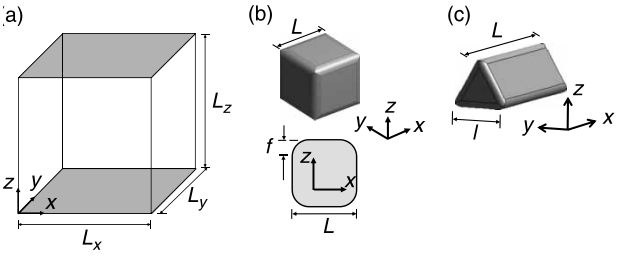

Figure 1. Schematic of (a) nematic cell, (b) cubic nanoparticle, and (c) equilateral triangular nanoprism.

alkanethiols [56]. When particles are not present in the system, the nematic in the cell exhibits a homogeneous texture in which its director field $\mathbf{n}(\mathbf{r})$ is aligned parallel to the z-axis. The insertion of particles produces strong variations in the director field and in the scalar order parameter $S(\mathbf{r})$, giving rise to the formation of topological defects around the particles due to the conflicting orientations imposed to the nematic by the homeotropic anchoring conditions at the surfaces.

In this study we considered two kinds of faceted nanoparticles, namely cubes and triangular prisms with rounded edges. The cubic particles have sides of length $L = 40\,\text{nm}$ with rounded edges of size $f = 5\,\text{nm}$ (Figure 1(b)). Equilateral triangular prisms were considered in this study; their rectangular faces have length $L = 150\,\text{nm}$, their triangular faces have sides of length $l = 68.7\,\text{nm}$ (Figure 1(c)), and their rounded edges have size $f = 5\,\text{nm}$. In this work we considered systems of one and two particles. For the case of a system with one cubic particle, the nanocube had its centre of mass placed in the centre of the simulation box. We rotated the particle around five of its 13 rotational symmetry axes, namely: (a) the x axis; (b) the axis $x = y = z$; (c) the axis $x = 0$, $y = z$; (d) the axis $y = 0$, $x = z$; and (e) the axis $z = 0$, $x = y$ (Figure 2(a)). For one non-spherical particle in a nematic, the most important variable determining the value of the free energy of the system is the relative orientation of the particle with respect to the director field $\mathbf{n}(\mathbf{r})$ far away from the particle. Based on the octahedral symmetry of a cube and how this symmetry is broken by the presence of a distinguished direction (i.e. the far-field director $\mathbf{n}(\mathbf{r})$, which is parallel to the z-axis), rotations of the cubic particle around the other eight rotational symmetry axes will lead to configurations similar to those found for the five rotations described above. For systems with two cubic particles, we have limited our analysis to particles where they approach each other *keeping a fixed orientation* equal to the most stable configuration found for the uniparticle systems. In consequence, when the two cubic particles are close to each other, two of their rounded edges are parallel to each other (Figure 5(a)). For the systems containing one cubic particle, a nematic cell with $L_x = L_y = L_z = 100\,\text{nm}$ was used; the dimensions of the nematic cell were $L_x = 130\,\text{nm}$, $L_y = 190\,\text{nm}$ and $L_z = 120\,\text{nm}$ for systems containing two nanocubes.

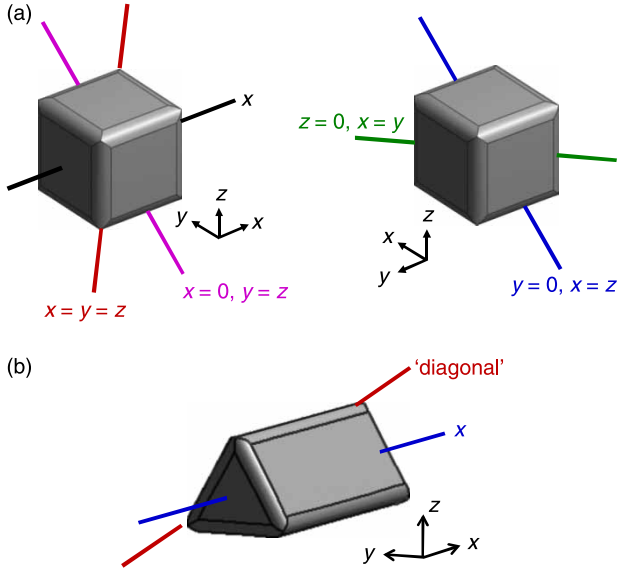

Figure 2. (Colour online). (a) A cubic nanoparticle immersed in a nematic was rotated around the five rotational symmetry axes indicated in the figure. (b) An equilateral triangular nanoprism in a nematic was rotated around the two rotational symmetry axes indicated in the figure. In all cases, the director field far away from the particle is parallel to the z-axis.

For systems with triangular prisms, the centres of the particles were always placed in the centre of the simulation box, in the plane $z = 0$. For systems with one equilateral triangular prism, we rotated the particle around the following two symmetry axes: (a) the x-axis; and (b) the axis that passes through two diagonal vertices of the two triangular faces (Figure 2(b)). All these rotations keep the long axis of the triangular prisms perpendicular to the director field $\mathbf{n}(\mathbf{r})$, which is parallel to the z-axis. We did not rotate our triangular prisms around the y-axis (which would eventually lead to an orientation where the long axis of the particle would be parallel to $\mathbf{n}(\mathbf{r})$), based on previous results for a system of one spherocylindrical particle with homeotropic anchoring at its surfaces immersed in a nematic [9]. In those studies it was found that a spherocylinder will adopt an orientation where its long axis is perpendicular to the director field $\mathbf{n}(\mathbf{r})$; a configuration where the spherocylinder has its long axis parallel to $\mathbf{n}(\mathbf{r})$ would suffer a large free energy penalty. On the other hand, rotations of the triangular prisms around other symmetry axes different from the ones considered here are expected to lead to results similar to those found for the rotations described above, since the far-field director $\mathbf{n}(\mathbf{r})$ is parallel to the z-axis. For systems with two triangular prisms, we limited our analysis to particles approaching each other *keeping their orientations fixed* and equal to the stable configurations found for the

uniparticle systems. Based on this premise and on the results obtained for one-particle systems, for the case of systems containing two triangular prisms we considered several particle arrays where the nanoprisms have their long axis oriented along the *x*-direction, but their centres are placed in different ways and the particle' orientations also differ. Specifically, for the case of systems with two equilateral triangular prisms we considered the following three particle arrays (Figure 9): (a) centres are on the *x*-axis and both particles have the same orientation (linear array); (b) centres are on the *y*-axis and both particles have the same orientation (parallel array); and (c) centres are on the *y*-axis, with one of the triangular prisms inverted with respect to the other one (inverted parallel array, see Figure 9(c)). For the systems containing one nanoprism, a nematic cell with $L_x = L_z = 1000\,\text{nm}$, $L_y = 500\,\text{nm}$ was used. For systems containing two nanoprisms, the dimensions of the nematic cell were $L_x = 400\,\text{nm}$, $L_y = 1200\,\text{nm}$ and $L_z = 300\,\text{nm}$ (parallel and inverted parallel arrays), and $L_x = 1200\,\text{nm}$, $L_y = 400\,\text{nm}$ and $L_z = 300\,\text{nm}$ (linear array).

2.2 *Mesoscale theory for the nematic LC*

The behaviour of the nematic was modelled using a mesoscale theory for the tensor order parameter $\mathbf{Q}(\mathbf{r})$; in contrast to the director field $\mathbf{n}(\mathbf{r})$, $\mathbf{Q}$ is free of discontinuities even at the LC defect cores. The scalar order parameter $S(\mathbf{r})$ and the director $\mathbf{n}(\mathbf{r})$ can be obtained from $\mathbf{Q}$ through its largest eigenvalue $2S/3$ and its associated eigenvector [28]. In previous studies of spherical nanoparticles in a nematic [8], results for the potentials of mean force (PMF) and the defect structures from the theory were compared with those from molecular simulations, where the nematic LC was modelled using Gay–Berne ellipsoids. Good agreement was found between both simulation procedures, down to nm-length scales comparable to the size of an LC molecule. Such a comparison provides a measure of the validity of the mesoscale theory even at nm-length scales. The theory corresponds to a particular case of the Beris–Edwards formulation of the thermodynamics of fluids with internal microstructure [57]. In this formulation, the evolution of the tensor order parameter $\mathbf{Q}$ as a function of position $\mathbf{r}$ and time t is determined by the functional derivative of the free energy F of the LC with respect to $\mathbf{Q}$:

$$\frac{\partial \mathbf{Q}}{\partial t} = -\frac{1}{\gamma}\left[\frac{\delta F}{\delta \mathbf{Q}} - \frac{1}{3}\mathrm{Tr}\left(\frac{\delta F}{\delta \mathbf{Q}}\right)\mathbf{I}\right], \tag{1}$$

where γ is a kinetic coefficient associated with the rotational viscosity of the nematic LC, and for simplicity it is assumed to be a constant. In Equation (1) it is assumed that $\delta F/\delta \mathbf{Q}$ has been symmetrised. The free energy F of the LC includes three contributions:

$$F = \int \mathrm{d}\mathbf{r} f_{\mathrm{LdG}}(\mathbf{r}) + \int \mathrm{d}\mathbf{r} f_{\mathrm{e}}(\mathbf{r}) + \oint dS f_{\mathrm{s}}(\mathbf{r}). \tag{2}$$

The first term, f_{LdG}, represents a Landau–de Gennes expansion [28] describing the short-range interactions that drive the bulk isotropic–nematic phase transition:

$$f_{\mathrm{LdG}} = \frac{A}{2}\left(1 - \frac{U}{3}\right)\mathrm{Tr}\left(\mathbf{Q}^2\right) - \frac{AU}{3}\mathrm{Tr}\left(\mathbf{Q}^3\right) + \frac{AU}{4}\left[\mathrm{Tr}\left(\mathbf{Q}^2\right)\right]^2. \tag{3}$$

The phenomenological coefficients A and U usually depend on the LC of interest. A controls the energy scale of the model, whereas U controls the value of the bulk scalar order parameter S:

$$S_{\mathrm{bulk}} = \frac{1}{4}\left(1 + 3\sqrt{1 - \frac{8}{3U}}\right). \tag{4}$$

In this model, the system is isotropic for $0 < U < 2.7$, and nematic for $U > 2.7$. The limits of metastability for the isotropic and nematic phases are $U = 3$ and 8/3, respectively. The third term in Equation (2) represents the surface contribution to the free energy, and accounts for the LC anchoring at the surfaces. We only consider the limit of infinitely strong homeotropic anchoring at all surfaces. In this limiting case, the prescribed perpendicular orientation of the LC at every surface must be satisfied, lest f_{s} diverges. In our calculations, the homeotropic anchoring of the LC at every surface is enforced through the boundary conditions.

The second term in Equation (2) describes the long-range elastic forces of the LC, and introduces a free energy penalty associated with gradients of the tensor order parameter field. For simplicity, in our calculations we have used the one-elastic-constant approximation [28], where the splay, twist and bend elastic constants K_{11}, K_{22} and K_{33} have a common value. In a previous simulation study considering spherocylindrical nanoparticles in a nematic LC [9], we obtained similar results for the defect structures and PMF when we used the one-elastic-constant approximation and a three-constant expression that is cubic in $\mathbf{Q}$ and its gradients [57–59]. The elastic free energy in the one-elastic-constant approximation takes the following form:

$$f_{\mathrm{e}} = \frac{L_1}{2}\frac{\partial Q_{ij}}{\partial x_k}\frac{\partial Q_{ij}}{\partial x_k}. \tag{5}$$

In Equation (5), $i, j, k \in x, y, z$, and the Einstein summation convention over repeated indexes is used. When the functional derivatives in Equation (1) are evaluated with Equations (2), (3) and (5), the following

system of partial differential equations for **Q** is obtained:

$$\frac{\partial Q_{ij}}{\partial t} = -\frac{1}{\gamma}\left\{A\left(1-\frac{U}{3}\right)Q_{ij} - AU\left[Q_{ik}Q_{kj} - \frac{\delta_{ij}}{3}Q_{kl}Q_{kl} - Q_{ij}(Q_{kl}Q_{kl})\right] - L_1\frac{\partial}{\partial x_k}\left(\frac{\partial Q_{ij}}{\partial x_k}\right)\right\}. \quad (6)$$

The system of partial differential equations given by Equation (6) was solved numerically for all the 3D systems considered in this study. The values of the dimensionless parameters are $A = 1$, $U = 6$, $\gamma = 400$ and $L_1 = 1$, corresponding to $S_{\text{bulk}} = 0.81$. Using suitable scaling factors for pressure (10^5 Pa), length (10 nm) and time (1 ns), these parameters correspond to a material having an elastic constant $K = 5$ pN (within the one-elastic-constant approximation), and an orientational viscosity of 0.04 Pa s. These values are representative of a low molecular-weight LC, such as 5CB (4-cyano-4′-pentylbiphenyl, CAS Registry Number 40817-08-1). In addition, from a dimensional analysis one can obtain a characteristic length scale, or nematic coherence length, for spatial variations of **Q** [60], which corresponds to $\xi = 17.3$ nm for our numerical parameters:

$$\xi = \sqrt{18L_1/AU}. \quad (7)$$

Equation (6) was solved for the five independent components of **Q** (Q_{xx}, Q_{yy}, Q_{xy}, Q_{xz} and Q_{yz}, since **Q** is traceless) using finite elements and the COMSOL Multiphysics™ package [61]. In order to solve the equations, we used the time-dependent algorithm DASPK, combined with the linear system solver GMRES and the incomplete LU preconditioner [61]. Equation (6) was solved for a sufficiently long time in order to observe negligible variations in the numerical solution with respect to time (i.e. a variation of $<0.2\%$ in the components of **Q** between successive time steps). Such a procedure corresponds to finding the solution that minimises the free energy (the right-hand side of Equation (6)). Following our previous studies [9,10,48], we performed 3D simulations using unstructured meshes containing tetrahedral, linear Lagrange elements automatically generated by COMSOL Multiphysics™ [62]. Different grid densities were used, and it was found that up to 51,865 finite elements were required for the numerical solutions to be independent of further mesh refinements. The mesh was significantly finer in the immediate vicinity of the walls and the nanoparticles, where important curvature effects and strong variations in **Q** are present. The minimum length of the finite elements in our finest grid size is $\sim 1.1 \times 10^{-4}$ l (for the case of cubic particles), which is comparable to those reported by Fukuda et al. [63] in their adaptive mesh refinement scheme. The initial conditions of **Q** in our simulations are such that the scalar order parameter S was initially fixed to the equilibrium value $S_{\text{bulk}} = 0.81$ (Equation (4)), and the director **n** is initially aligned along the z direction. We repeated some of our calculations starting from the LC in an isotropic phase, and we obtained similar results. The scalar order parameter at the nanoparticles' surface was also set to $S = S_{\text{bulk}} = 0.81$.

Different methods are available to depict the NLC defect structures (the regions where the nematic director field becomes discontinuous) [64,65]. In this work, we follow previous literature studies [8–10,48] and adopt the contour $S = 0.30$ to visualise defects in 3D, since it is approximately the smallest value of scalar order parameter for a stable bulk nematic in our particular model [57,60]. The free energy values used in the computation of the PMF were determined by numerical integration of Equations (2), (3) and (5) over the volume of the system.

3. Results and discussion

3.1 Cubic particles

In this section we present results for systems of one and two cubic particles. We first present results for the PMF and defect structures observed when a cubic nanoparticle immersed in a nematic is rotated around five of its symmetry axes. The cubic nanoparticle was centred in the origin (0,0,0), and was rotated an angle θ around five of its 13 rotational symmetry axes, namely: (a) the x axis; (b) the axis $x = y = z$; (c) the axis $x = 0$, $y = z$; (d) the axis $y = 0$, $x = z$; and (e) the axis $z = 0$, $x = y$ (Figure 2(a)). As mentioned before, for one non-spherical particle in a nematic the most important variable determining the value of the free energy of the system is the relative orientation of the particle with respect to the far-field director **n**(**r**). As **n**(**r**) is parallel to the z-axis far away from the particle, rotations of the cube around the other eight symmetry axes should lead to configurations and defect structures similar to those found for the five rotations mentioned before. Results for the PMF when the particle rotates around these symmetry axes are presented in Figure 3. For any given particle rotation, the PMF was calculated as the difference in free energy with respect to that for the case of $\theta = 0°$. In Figure 4 we present 3D visualisations of the defect structures formed by the nematic, when the system is in its reference state ($\theta = 0°$), and when the system is at a minimum in the PMF for the rotation axes considered in this work.

At the reference state ($\theta = 0°$, Figure 3), the defect structure consists of a distorted Saturn ring that surrounds most of the area of the four lateral faces of the cube (Figure 4(a)). The defect core does not cover either the top and bottom faces, or the rounded corners between these two faces and the lateral ones. When the particle rotates around the x axis, it reaches a minimum of $\sim -85k_BT$ in the PMF at $\theta \sim 45°$ (Figure 3). In this state, the defect

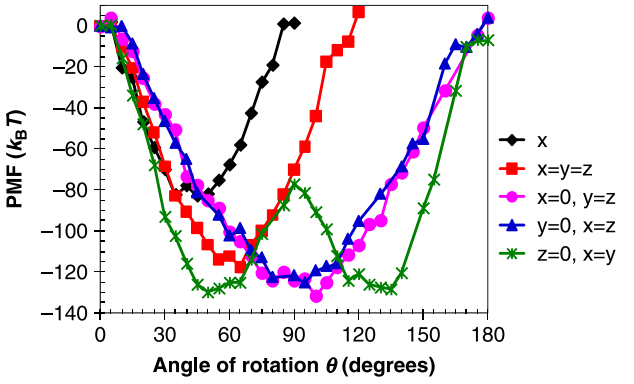

Figure 3. (Colour online). PMF for a cubic nanoparticle rotating around the following symmetry axes: (1) the x axis; (2) the axis $x = y = z$; (3) the axis $x = 0$, $y = z$; (4) the axis $y = 0$, $x = z$; and (5) the axis $z = 0$, $x = y$.

structure is a distorted Saturn ring consisting of four parts: two narrow sections covering two of the rounded edges of the cube, and two wide sections covering most of the area of the two lateral faces of the cube that are perpendicular to

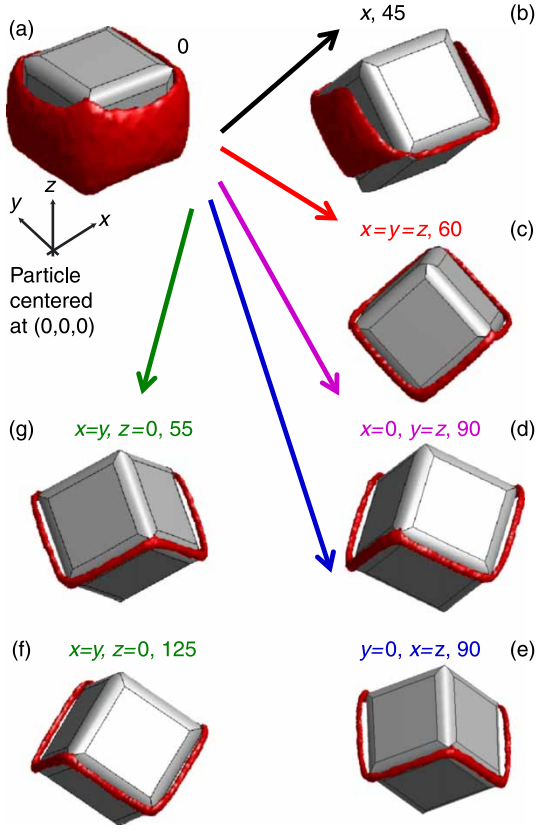

Figure 4. (Colour online). 3D visualisations of the defect structures formed by the nematic around a cubic nanoparticle at its reference state ($\theta = 0°$), and at the minimum of the PMF (Figure 3) for the rotations of the cubic particle around the five symmetry axes considered in this study.

$\mathbf{n}(\mathbf{r}) \| z$ (Figure 4(b)). Rotation of the cubic particle around the other four symmetry axes considered (i.e., $x = y = z$; $x = 0$, $y = z$; $y = 0$, $x = z$; and $z = 0$, $x = y$) leads to PMF curves that exhibit similar values at their minima ($\sim -125 k_B T$), which suggests that these configurations have similar thermodynamic stability. The defect structures found at these minima ($\theta \sim 60°$ around $x = y = z$; $\theta \sim 90°$ around $x = 0$, $y = z$ and $y = 0$, $x = z$; and $\theta \sim 55°$ and $\theta \sim 125°$ around $z = 0$, $x = y$) are indeed very similar, consisting of a distorted Saturn ring with sharp bends, covering six of the rounded edges of the cubic nanoparticle (Figure 4(c)–(g)). The PMF of these four configurations ($\sim -125 k_B T$) is significantly lower than the value found at the minimum of the PMF curve when the particle rotates around the x axis ($\sim -85 k_B T$). These results are consistent with the fact that rotations around the three latter symmetry axes lead to defect structures that exhibit smaller surface areas (Figure 4(c)–(g)), as compared to those observed when the particle rotates around the x axis (Figure 4(b)).

For the two-nanocube systems, we have decided to limit our analysis to cubic particles that are rotated an angle of $\theta = 125°$ with respect to the axis $z = 0$, $x = y$ (Figure 4(f)), which corresponds to the most stable configuration for rotations around that symmetry axis (Figure 3). Results for the PMF obtained when two cubic nanoparticles approach each other *while keeping their orientations fixed* are presented in Figure 5(b). In Figure 5(a) we present 3D visualisations of the defect structures obtained when the particles are far apart, and when the particles are at the minimum of the PMF. The particles approach each other in a direction such that one of the six defect cores formed around one cube, could be in direct contact with a defect core from the other cube when the particles are close together (Figure 5(a)). When the particles are separated by a small distance $d = 4$ nm, the nematic forms a defect structure where a new disclination ring forms in the interparticle space. A similar defect structure was first reported for spherical particles in the computational study of Guzmán et al. [8], and was later observed in other computational studies for spherical [6c,45] and spherocylindrical [9,48] particles. Such a defect structure was also observed experimentally for micron-sized spheres by Ravnik et al. [6c], who termed it an 'entangled hyperbolic' defect structure. The distorted 'entangled hyperbolic' defect structure that formed when cubic nanoparticles are close to each other has a free energy that is $\sim -85 k_B T$ more stable than the free energy exhibited by a configuration where the cubes are far apart. As a comparison, a pair of nanospheres with comparable diameter forming an 'entangled hyperbolic' defect structure exhibits a PMF minimum of $\sim -110 k_B T$ [8c]; furthermore, spherocylindrical nanoparticles that are close to each other with their long axes parallel are expected to show even deeper PMF minima [9,48]. As discussed in [9], the magnitude of the PMF

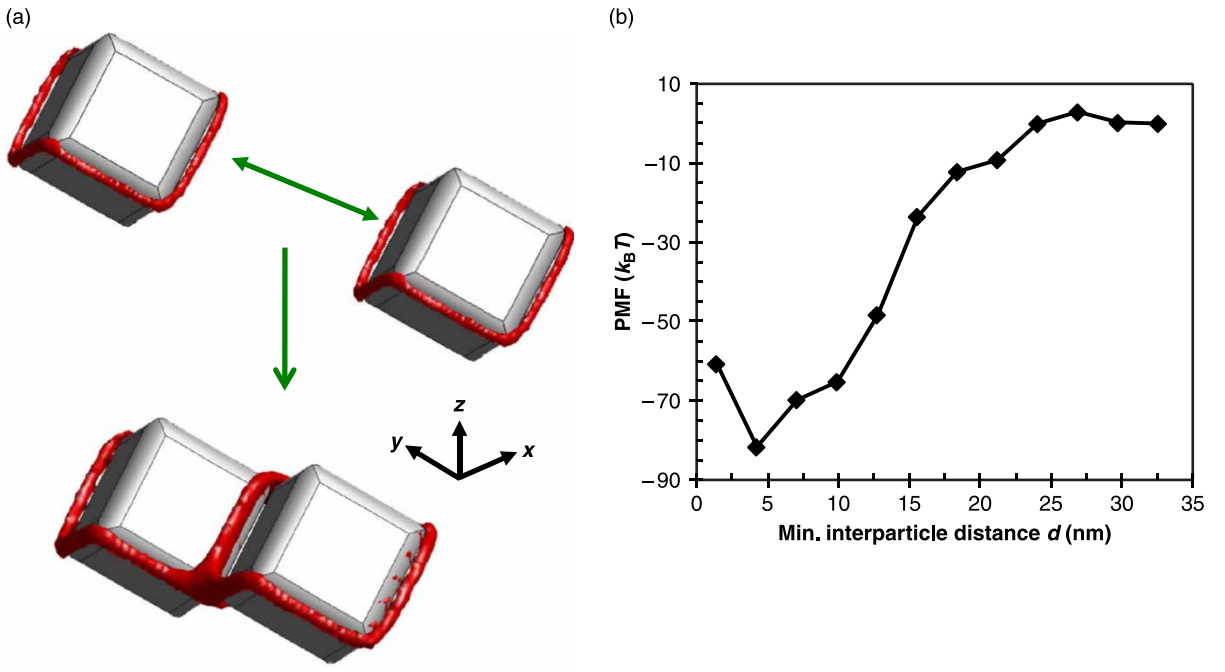

Figure 5. (Colour online). (a) 3D visualisations of the 'entangled hyperbolic' defect structures formed by a nematic around two cubic nanoparticles when the particles are far apart, and when the particles are separated by a distance d corresponding to the minimum of the PMF (Figure 5(b)). The two nanoparticles approach each other *while keeping their orientations fixed*. (b) PMF as a function of the minimum surface-to-surface interparticle distance d, for two nanocubes approaching each other.

minima depends on factors such as curvature effects in the interparticle region, as well as the size of the 'hole' of the interparticle disclination ring. The interparticle region is filled by a few layers of molecules of LC in a highly-ordered nematic that 'bridges' the nanoparticles together. The size of the 'hole' in the interparticle disclination ring is significantly smaller for the case of a pair of cubic nanoparticles (Figure 5(a)) as compared to those observed for two spherical and two spherocylindrical particles (see, e.g. Figures 2 and 6 in [8a,9], respectively). In addition, the effects of curvature involving the rounded edges of the two nanocubes (which are in close proximity in the interparticle region) are more important than the effects observed for the case of two spheres and two parallel spherocylinders.

3.2 *Triangular prisms*

In this section we present results for systems of equilateral triangular prisms immersed in a nematic. We first present results for the PMF and defect structures observed when one triangular prism, placed in the centre of the simulation box (i.e. the plane $z = 0$) and with its long axis parallel to the x-axis, is rotated around the following two symmetry axes: (a) the x-axis; and (b) the axis that passes through two of the corners of the equilateral triangular prism (Figure 2(b)). Results for the PMF as a function of the angle of rotation θ are presented in Figure 6. For any given particle rotation around any of these two axes, the PMF was calculated as the difference in free energy with respect to a common reference state, where the prism has an orientation such that one of its rectangular faces has a normal vector equal to $(0, 0, -1)$. This reference state corresponds to $\theta = 0^\circ$ for the two rotation axes considered

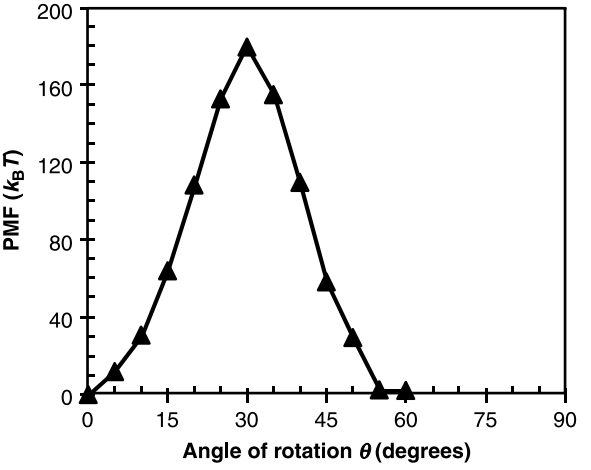

Figure 6. (Colour online). PMF for an equilateral triangular nanoprism rotating around the x-axis. Results for the rotation of the nanoprism around the axis that passes through two diagonal vertices of the two triangular faces Figure 2(b) are not depicted since they are equivalent to those obtained upon rotation around the x-axis.

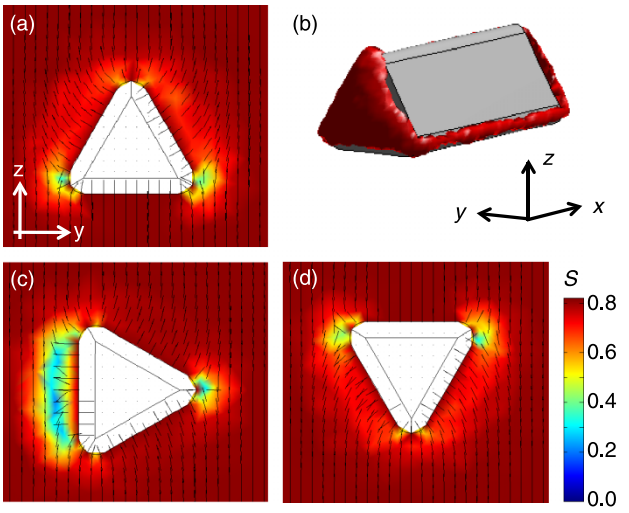

Figure 7. (Colour online). Contour maps of the scalar order parameter S superimposed with the director field in the y–z plane for (a) $\theta = 0°$, (c) $\theta = 30°$, and (d) $\theta = 60°$. A 3D visualisation of the defect structure for $\theta = 0°$ is presented in (b).

in this study, and is depicted in Figure 7(a),(b). The free energy of such a common reference state was arbitrarily set to zero. As mentioned before, for a non-spherical particle in a nematic the most important factor determining the value of the free energy of the system is the relative orientation of the particle with respect to the far-field director $\mathbf{n}(\mathbf{r})$. In particular, rotations of an equilateral triangular prism around the two symmetry axes mentioned above lead to particle configurations that have similar orientations with respect to the far-field director $\mathbf{n}(\mathbf{r}) \| z$, and thus we only show PMF results for rotations of the triangular nanoprism around the x-axis. Our PMF results for the rotation of one equilateral triangular nanoprism suggest that the most stable configuration corresponds to those with angles $\theta = 0°$ and $\theta = 60°$. In fact, these two configurations are completely equivalent, as it can be seen in Figure 7(a),(d), where we present contour maps of the scalar order parameter S in different planes, for $\theta = 0°$ and $\theta = 60°$; the corresponding director fields are superimposed to these maps. In Figure 7(b) we also present a 3D visualisation of the defect structure formed by the nematic around the particle for the case of $\theta = 0°$. The defect structure formed by the nematic in this case consists of two large disclination regions covering the two triangular faces of the prism, which are oriented parallel to the far-field director $\mathbf{n}(\mathbf{r})$; the nematic also forms two narrow disclination regions surrounding two of the rounded edges of the prism (Figure 7(a),(b)). Defect structures with smaller surface areas are preferred since they lead to lower values of free energies. For example, the contour map for $\theta = 30°$ (Figure 7(c)) suggests that for this angle, the defect structure consists of a large disclination region covering most of the area of one of the rectangular faces of the prism; as a result the PMF curves exhibit maxima at $\theta = 30°$ (Figure 6).

For systems with two equilateral triangular prisms, as mentioned before we limited our analysis to particles approaching each other *keeping their orientations fixed* and equal to the stable configurations found for the uniparticle systems. Therefore, we considered several particle arrays where the nanoprisms have their long axis oriented along the x-direction, but their centres are placed in different ways and the particle' orientations also differ. Specifically, for the case of systems with two equilateral triangular prisms we considered the following three particle arrays (Figure 9): (a) linear array, where the particles' centres are on the x-axis and both particles have the same orientation (corresponding to $\theta = 0°$ in Figure 7); (b) parallel array, where the particles' centres are on the y-axis and both particles have the same orientation (corresponding to $\theta = 0°$ in Figure 7); and (c) inverted parallel array (Figure 9(e)), where the particles' centres are on the y-axis, and one of the triangular prisms is inverted with respect to the other one (i.e. one of the particles has $\theta = 0°$ and the second has $\theta = 60°$ in Figure 7). The PMF was determined as a function of the minimum surface-to-surface interparticle distance d, and these results are presented in Figure 8. In this case, the PMF represents the difference in free energy for any given two-particle configuration, with respect to a situation where they are infinitely apart.

Our results for two equilateral triangular prisms in a parallel array indicate that when the distance d is reduced to about 60 nm, the PMF first becomes slightly positive, suggesting that the particles first experience a repulsion as they approach each other. Such a repulsion was also found in other experimental [6e] and computational studies [6e,8,32] considering spherical particles in a nematic. These

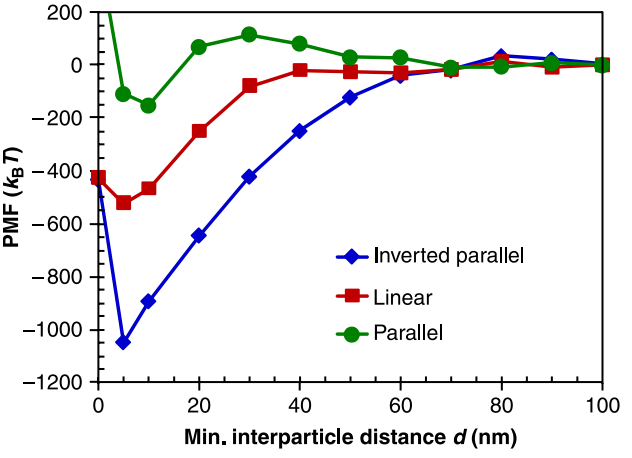

Figure 8. (Colour online). PMF as a function of the minimum surface-to-surface interparticle distance d, for two nanoprisms approaching each other in a parallel, linear and inverted parallel array (see Figure 9).

results also suggest that this initial repulsion decreases in magnitude as the particle size is reduced. Moreover, experimental and numerical results [6e] indicate that this repulsion is observed only when both spherical particles approach each other along a plane containing both Saturn rings entirely. This repulsion can be avoided by making one of the spheres to approach the other via an off-centre trajectory (i.e. making one of the particles to leave the plane $z = 0$ and then come back to this plane at interparticle distances small enough; see, e.g. Figure 1 in [6e]). The total PMF for a pair of triangular prisms in a parallel array becomes negative as $d < 20\,\text{nm}$ for a parallel array, reaching a minimum of about $-150k_BT$ at $d = 10\,\text{nm}$. At this distance, the nematic forms a defect structure consisting of one large disclination ring forming in the interparticle space, and fused to the original defect structures formed around each particle (Figure 9(a),(b)). Such a defect structure resembles the 'entangled hyperbolic' defect structure observed for pairs of particles with spherical [6c,8,45], spherocylindrical [9,48] and cubic shape (this work). Our PMF results for the other particle arrays considered in this study (linear and inverted parallel) follow the same trends described before for the parallel array: as d is reduced the PMF first becomes positive, and further reductions in d makes the PMF to become negative. In these two arrays the initial repulsion is significantly smaller and is observed at larger values of d as compared to the parallel array of nanoprisms. Furthermore, the minima observed in the PMF curves (Figure 8) for the linear ($\sim -525k_BT$) and inverted parallel arrays ($\sim -1050k_BT$) are significantly larger than that observed for the parallel array ($\sim -150k_BT$). Such an observation can be explained by depicting the defect structures formed by the nematic around the particles (Figure 9). A linear array of triangular prisms 'shares' a common triangular disclination region in the interparticle space, and has a size equivalent to the area of a triangular face of the prisms (Figure 9(b)). On the other hand, an inverted parallel array exhibits a more compact defect structure, consisting of two large disclination regions covering the four triangular faces of the two prisms; there are also four narrow disclination regions covering four of the rounded edges of the two prisms (Figure 9(c)). Visual inspection of the structures shown in Figure 9 suggests that the total area of the defect structure around a parallel array of triangular prisms is significantly larger than the area of the defects formed around linear and inverted parallel arrays of the same nanoprisms. Defect structures with smaller areas usually exhibit smaller values of free energy and are thus more stable from a thermodynamic point of view. Furthermore, an inverted parallel array exhibits a more

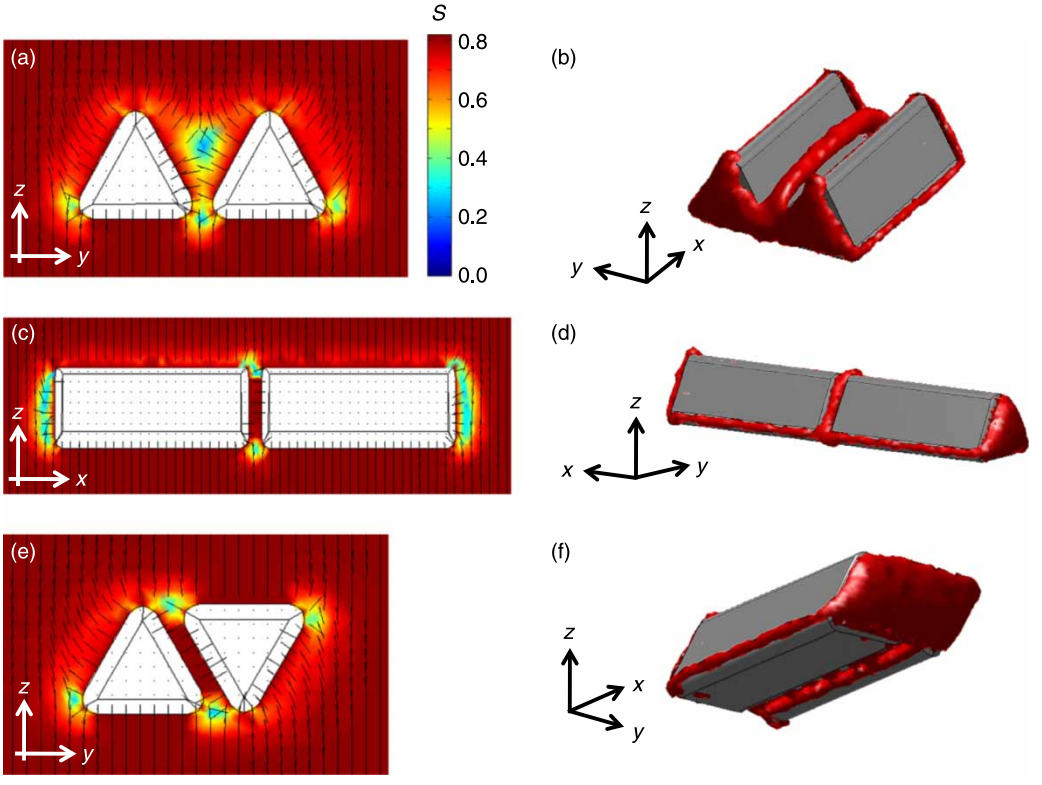

Figure 9. (Colour online). Contour maps of the scalar order parameter S superimposed with the director field in different planes (left) and 3D visualisations of the defect structures formed by a nematic around two triangular nanoprisms in (a),(b) parallel array; (c),(d) linear array; and (e),(f) inverted parallel array. These visualisations correspond to points close to the minima in the PMF (Figure 8).

compact defect structure than a linear array of nanoprisms, and thus the PMF minimum in the former array is deeper than in the linear array. Just for comparison purposes, the minimum in the PMF observed for a pair of nanospheres with a diameter $D = 28\,\text{nm}$ (comparable to the size of the triangular faces of our nanoprisms) is $\sim -73k_BT$ [8c] when the spheres are in close proximity. The minima observed in our arrays of nanoprisms are significantly larger than that observed for nanospheres of similar diameters. There is no data available for pairs of spherocylinders with similar sizes; however, for pairs of spherocylinders that are close to each other with their long axes parallel, the PMF minima are $\sim -80k_BT$ ($D = 12.4\,\text{nm}$, $L = 37.2\,\text{nm}$) [9] and $\sim -5500k_BT$ ($D = 100\,\text{nm}$, $L = 300\,\text{nm}$) [48]. The PMF minima observed for our different arrays of triangular prisms are between these numerical ranges.

Our results suggest that the LC-mediated interactions between pairs of particles are strong and anisotropic, and vary with the shape and dimensions of the particles. These interactions can be used to bind the particles together and assemble them into ordered structures with unconventional morphologies. As an example, in Figure 10(a) we depict an ordered structure that could be assembled using cubic particles immersed in a nematic LC 'sandwiched' between two parallel walls forming a thin cell. The particles would be held together in such an ordered structure by the defects formed by the nematic around the cubic particles. Such an ordered structure could be assembled in principle following the same ideas of the work presented by Muševič et al. [6] for the assembly of spherical and spherocylindrical particles in a nematic. Similarly, ordered structures formed by a number of triangular nanoprisms arranged in linear and inverted parallel arrays could also be assembled (Figure 10(b)). Ordered particle structures with symmetries different from the hexagonally close-packed crystals typically formed by spherical colloids could be relevant for applications in photonics and nanoscale optoelectronics [49,55].

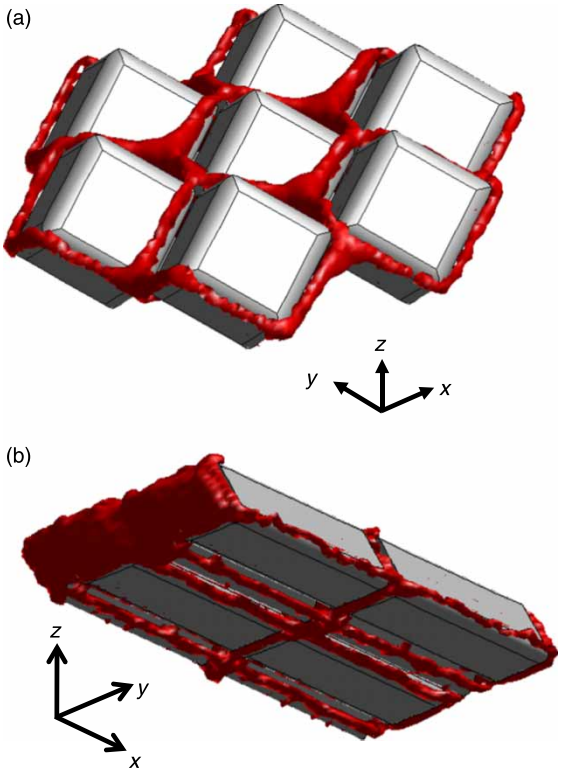

Figure 10. (Colour online). Representation of ordered structures that could be assembled using (a) cubic particles, and (b) equilateral triangular prisms, immersed in a nematic LC. The particles are held together by the defects formed by the nematic around the particles.

4. Concluding remarks

We have investigated the defect structures and the PMF that arise when faceted nanoparticles, namely cubes and triangular prisms, are immersed in a nematic LC. Using a mesoscale theory for the tensor order parameter **Q** of the nematic, we analysed different configurations with one and two faceted nanoparticles with strong homeotropic anchoring at their surfaces. When one nanocube ($L = 40\,\text{nm}$) is rotated around several of its symmetry axes (Figure 2), the most stable defect structure consists of a distorted Saturn ring exhibiting six discontinuous sections, each one covering 6 of the 12 rounded edges of the cube (Figure 4). We then made two nanocubes approach each other in a way that two of the discontinuous defect cores (each belonging to a different particle) could be in direct contact when the particles are close (Figure 5(a)). When the two cubic nanoparticles are close to each other, the nematic forms a distorted 'entangled hyperbolic' defect structure around the particles, corresponding to a PMF minimum of $\sim -85k_BT$. In comparison, a PMF minimum of $\sim -110k_BT$ has been observed for the case of an 'entangled hyperbolic' defect structure around spherical nanoparticles of comparable size [8c]; and a similar defect structure formed around spherocylinders of comparable diameters that are close to each other with their long axes parallel exhibits even deeper PMF minima [9,48].

Our results for systems of one equilateral triangular nanoprism ($l = 68.7\,\text{nm}$, $L = 150\,\text{nm}$) indicate that the most stable configuration is achieved when the prism is placed with its long axis perpendicular to the far-field director $\mathbf{n}(\mathbf{r})$, and the normal vector of one of its rectangular faces is parallel to the far-field director (Figure 7). For such a configuration, the defect structure formed by the nematic consists of two large disclination regions covering the two triangular faces of the prism, and two narrow disclination regions surrounding two of the rounded edges of the prism (Figure 7). For systems of two nanoprisms having their long axes perpendicular to the far-field director, our results suggest that inverted parallel arrays (Figure 9(e),(f)) are

thermodynamically more stable than linear arrays (Figure 9(c),(d)), which in turn are more stable than parallel arrays (Figure 9(a),(b)). The minima observed in the PMF curves for the linear ($\sim -525k_BT$) and inverted parallel arrays ($\sim -1050k_BT$) are significantly deeper than that observed for the parallel array ($\sim -150k_BT$). In comparison, a pair of nanospheres with a diameter $D = 28$ nm (comparable to the size of the triangular faces of our nanoprisms) has a PMF minimum of $\sim -73k_BT$ [8c] when the spheres are in close proximity. Our results also suggest that defect structures with smaller surface areas tend to exhibit lower values of free energy and thus are thermodynamically more stable.

In this work we have only evaluated the changes in the free energy of the system for different configurations of faceted nanoparticles immersed in a nematic LC. Due to the non-spherical shape of the particles, the nematic is expected to transmit torques to the nanoparticles, which can induce different effects [28,48,66] not considered in this work. Although these torques can be estimated using the models and methods presented in this paper, the calculation of these torques is beyond the scope of the work presented here due to its extension, and will be the subject of our future studies. Our results suggest that the LC-mediated interactions between pairs of particles are strong and anisotropic, and vary with the shape and dimensions of the particles. These interactions can be used to bind the particles together and assemble them into ordered structures with unconventional morphologies. Particles with unique shapes, as well as 'patterned' particles (e.g. Janus spheres, gold-platinum rods, etc. see, e.g. [49b]) are readily available. For the case of particles with chemical patterns introducing some degree of chirality, if the different particles' regions induce a nematic to anchor in different directions (homeotropic, planar), in principle one could assemble ordered particle structures exhibiting some degree of chirality even though the nematic is achiral. We are currently studying the physics of particles with non-spherical shapes and surface patterns when they are immersed in LCs. These studies could allow us to determine the properties (e.g., morphology, type of symmetry, etc.) of the structures that could be assembled using these types of particles. These results could be relevant for ongoing research in light-scattering devices, electro-optical switches, photonics, nanoscale electronics, displays and optical sensors.

References

[1] (a) P. Poulin, H. Stark, T.C. Lubensky, and D.A. Weitz, *Novel colloidal interactions in anisotropic fluids*, Science 275 (1997), pp. 1770–1773; (b) P. Poulin, V. Cabuil, and D.A. Weitz, *Direct measurement of colloidal forces in an anisotropic solvent*, Phys. Rev. Lett. 79 (1997), pp. 4862–4865; (c) P. Poulin and D.A. Weitz, *Inverted and multiple nematic emulsions*, Phys. Rev. E 57 (1998), pp. 626-637; (d) J.C. Loudet, P. Barois, and P. Poulin, *Colloidal ordering from phase separation in a liquid crystalline continuous phase*, Nature 407 (2000), pp. 611–613.

[2] (a) V.G. Nazarenko, A.B. Nych, and B.I. Lev, *Crystal structure in nematic emulsion*, Phys. Rev. Lett. 87 (2001), 075504; (b) I.I. Smalyukh, S. Chernyshuk, B.I. Lev, A.B. Nych, U. Ognysta, V.G. Nazarenko, and O.D. Lavrentovich, *Ordered droplet structures at the liquid crystal surface and elastic-capillary colloidal interactions*, Phys. Rev. Lett. 93 (2004), 117801.

[3] (a) M. Yada, J. Yamamoto, and H. Yokoyama, *Spontaneous formation of regular defect array in water-in-cholesteric liquid crystal emulsions*, Langmuir 18 (2002), pp. 7436–7440; (b) M. Yada, J. Yamamoto, and H. Yokoyama, *Direct observation of anisotropic interparticle forces in nematic colloids with optical tweezers*, Phys. Rev. Lett. 92 (2004), 185501.

[4] (a) A.B. Nych, U.M. Ognysta, V.M. Pergamenshchik, B.I. Lev, V.G. Nazarenko, I. Muševič, M. Škarabot, and O.D. Lavrentovich, *Coexistence of two colloidal crystals at the nematic-liquid-crystal-air interface*, Phys. Rev. Lett. 98 (2007), 057801; (b) U. Ognysta, A. Nych, V. Nazarenko, I. Muševič, M. Škarabot, M. Ravnik, S. Žumer, I. Poberaj, and D. Babič, *2D interactions and binary crystals of dipolar and quadrupolar nematic colloids*, Phys. Rev. Lett. 100 (2008), 217803.

[5] K. Kita, M. Ichikawa, and Y. Kimura, *Self-assembly of polymer droplets in a nematic liquid crystal at phase separation*, Phys. Rev. E 77 (2008), 041702.

[6] (a) I. Muševič, M. Škarabot, U. Tkalec, M. Ravnik, and S. Žumer, *Two-dimensional nematic colloidal crystals self-assembled by topological defects*, Science 313 (2006), pp. 954–958; (b) M. Škarabot, M. Ravnik, S. Žumer, U. Tkalec, I. Poberaj, D. Babič, N. Osterman, and I. Muševič, *Two-dimensional dipolar nematic colloidal crystals*, Phys. Rev. E 76 (2007), 051406; (c) M. Ravnik, M. Škarabot, S. Žumer, U. Tkalec, I. Poberaj, D. Babič, N. Osterman, and I. Muševič, *Entangled nematic colloidal dimers and wires*, Phys. Rev. Lett. 99 (2007), 247801; (d) M. Škarabot, M. Ravnik, S. Žumer, U. Tkalec, I. Poberaj, D. Babič, N. Osterman, and I. Muševič, *Interactions of quadrupolar nematic colloids*, Phys. Rev. E 77 (2008), 031705; (e) M. Škarabot, M. Ravnik, S. Žumer, U. Tkalec, I. Poberaj, D. Babič, and I. Muševič, *Hierarchical self-assembly of nematic colloidal superstructures*, Phys. Rev. E 77 (2008), 061706; (f) U. Tkalec, M. Škarabot, and I. Muševič, *Interactions of micro-rods in a thin layer of a nematic liquid crystal*, Soft Matter 4 (2008), pp. 2402–2409.

[7] K. Takahashi, M. Ichikawa, and Y. Kimura, *Force between colloidal particles in a nematic liquid crystal studied by optical tweezers*, Phys. Rev. E 77 (2008), 020703.

[8] (a) O. Guzmán, E.B. Kim, S. Grollau, N.L. Abbott, and J.J. de Pablo, *Defect structure around two colloids in a liquid crystal*, Phys. Rev. Lett. 91 (2003), 235507; (b) S. Grollau, E.B. Kim, O. Guzmán, N.L. Abbott, and J.J. de Pablo, *Monte Carlo simulations and dynamic field theory for suspended particles in liquid crystalline systems*, J. Chem. Phys. 119 (2003), pp. 2444–2455; (c) E.B. Kim, O. Guzmán, S. Grollau, N.L. Abbott, and J.J. de Pablo, *Interactions between spherical colloids mediated by a liquid crystal: a molecular simulation and mesoscale study*, J. Chem. Phys. 121 (2004), pp. 1949–1961; (d) O. Guzmán, N.L. Abbott, and J.J. de Pablo, *Anisotropic nanoparticles immersed in a nematic liquid crystal*, J. Polym. Sci. Polym. Phys. 43 (2005), pp. 1033–1040.

[9] F.R. Hung, O. Guzmán, B.T. Gettelfinger, N.L. Abbott, and J.J. de Pablo, *Anisotropic nanoparticles immersed in a nematic liquid crystal: defect structures and potentials of mean force*, Phys. Rev. E 74 (2006), 011711.

[10] F.R. Hung, B.T. Gettelfinger, G.M. Koenig Jr., N.L. Abbott, and J.J. de Pablo, *Nanoparticles in nematic liquid crystals: interactions with nanochannels*, J. Chem. Phys. 127 (2007), 124702.

[11] (a) T. Hegmann, H. Qi, and V.M. Marx, *Nanoparticles in liquid crystals: synthesis, self-assembly, defect formation and potential applications*, J. Inorg. Organomet. Polym. Mater. 17 (2007), pp. 483–508; (b) H. Qi and T. Hegmann, *Impact of nanoscale particles and carbon nanotubes on current and future generations of liquid crystal displays*, J. Mater. Chem. 18 (2008), pp. 3288–3294.

[12] (a) H. Qi and T. Hegmann, *Formation of periodic stripe patterns in nematic liquid crystals doped with functionalized gold nanoparticles*, J. Mater. Chem. 16 (2006), pp. 4197–4205; (b) H. Qi, A. Lepp,

P.A. Heiney, and T. Hegmann, *Effects of hydrophilic and hydrophobic gold nanoclusters on the stability and ordering of bolaamphiphilic liquid crystals*, J. Mater. Chem. 17 (2007), pp. 2139–2144.

[13] M. Mitov, C. Bourgerette, and F. de Guerville, *Fingerprint patterning of solid nanoparticles embedded in a cholesteric liquid crystal*, J. Phys.: Condens. Matter 16 (2004), pp. S1981–S1988.

[14] M.C.W. van Boxtel, R.H.C. Janssen, D.J. Broer, H.T.A. Wilderbeek, and C.W.M. Bastiaansen, *Polymer-filled nematics: a new class of light-scattering materials for electro optical switches*, Adv. Mater. 12 (2000), pp. 753–757.

[15] S.R. Nersisyan and N.V. Tabiryan, *The effect of low-frequency microvibrations on nanoparticle networks embedded in liquid crystals*, Appl. Phys. Lett. 88 (2006), 151106.

[16] P.A. Kossyrev, A. Yin, S.G. Cloutier, D.A. Cardimona, D. Huang, P.M. Alsing, and J.M. Xu, *Electric field tuning of plasmonic response of nanodot array in liquid crystal matrix*, Nano Lett. 5 (2005), pp. 1978–1981.

[17] C. Lapointe, A. Hultgren, D.M. Silevitch, E.J. Felton, D.H. Reich, and R.L. Leheny, *Elastic torque and the levitation of metal wires by a nematic liquid crystal*, Science 303 (2004), pp. 652–655.

[18] (a) M.D. Lynch and D.L. Patrick, *Organizing carbon nanotubes with liquid crystal*, Nano Lett. 2 (2002), pp. 1197–1201; (b) M.D. Lynch and D.L. Patrick, *Controlling the orientation of micron-sized rod-shaped SiC particles with nematic liquid crystal solvents*, Chem. Mater. 16 (2004), pp. 762–767.

[19] I. Dierking, G. Scalia, P. Morales, and D. LeClere, *Aligning and reorienting carbon nanotubes with nematic liquid crystals*, Adv. Mater. 16 (2004), pp. 865–869.

[20] P. van der Schoot, V. Popa-Nita, and S. Kralj, *Alignment of carbon nanotubes in nematic liquid crystals*, J. Phys. Chem. B 112 (2008), pp. 4512–4518.

[21] (a) V.K. Gupta, J.J. Skaife, T.B. Dubrovsky, and N.L. Abbott, *Optical amplification of ligand-receptor binding using liquid crystals*, Science 279 (1998), pp. 2077–2080; (b) R.R. Shah and N.L. Abbott, *Principles for measurement of chemical exposure based on recognition-driven anchoring transitions in liquid crystals*, Science 293 (2001), pp. 1296–1299; (c) J.M. Brake, M.K. Daschner, Y.Y. Luk, and N.L. Abbott, *Biomolecular interactions at phospholipid-decorated surfaces of liquid crystals*, Science 302 (2003), pp. 2094–2097; (d) G.M. Koenig Jr., M.-V. Meli, J.-S. Park, J.J. de Pablo, and N.L. Abbott, *Coupling of the plasmon resonances of chemically functionalized gold nanoparticles to local order in thermotropic liquid crystals*, Chem. Mater. 19 (2007), pp. 1053–1061; (e) G.M. Koenig Jr., B.T. Gettelfinger, J.J. de Pablo, and N.L. Abbott, *Using localized surface plasmon resonances to probe the nanoscopic origins of adsorbate-driven ordering transitions of liquid crystals in contact with chemically functionalized gold nanodots*, Nano Lett. 8 (2008), pp. 2362–2368.

[22] E. Tjipto, K.D. Cadwell, J.F. Quinn, A.P.R. Johnston, N.L. Abbott, and F. Caruso, *Tailoring the interfaces between nematic liquid crystal emulsions and aqueous phases via layer-by-layer assembly*, Nano Lett. 6 (2006), pp. 2243–2248.

[23] S.V. Shiyanovskii, T. Schneider, I.I. Smalyukh, T. Ishikawa, G.D. Niehaus, K.J. Doane, C.J. Woolverton, and O.D. Lavrentovich, *Real-time microbe detection based on director distortions around growing immune complexes in lyotropic chromonic liquid crystals*, Phys. Rev. E 71 (2005), 020702 (R).

[24] J. Müller, C. Sönnichsen, H. von Poschinger, G. von Plessen, T.A. Klar, and J. Feldmann, *Electrically controlled light scattering with single metal nanoparticles*, Appl. Phys. Lett. 81 (2002), pp. 171–173.

[25] (a) S. Grollau, O. Guzmán, N.L. Abbott, and J.J. de Pablo, *Slow dynamics of thin nematic films in the presence of adsorbed nanoparticles*, J. Chem. Phys. 122 (2005), 024703; (b) O. Guzmán, N.L. Abbott, and J.J. de Pablo, *Quenched disorder in a liquid-crystal biosensor: adsorbed nanoparticles at confining walls*, J. Chem. Phys. 122 (2005), 184711.

[26] D.K. Hwang and A.D. Rey, *Optical modeling of liquid crystal biosensors*, J. Chem. Phys. 125 (2006), 174902.

[27] R. Mohanraj and H.L. Wu, *Simulation of dynamics of a nematic liquid crystal for a biosensor application*, Sensor Lett. 5 (2007), pp. 538–551.

[28] P.G. de Gennes and J. Prost, *The Physics of Liquid Crystals*, 2nd ed., Clarendon, Oxford, 1993.

[29] H. Stark, *Physics of colloidal dispersions in nematic liquid crystals*, Phys. Rep. 351 (2001), pp. 387–474.

[30] O. Mondain-Monval, J.C. Dedieu, T. Gulik-Krzywicki, and P. Poulin, *Weak surface energy in nematic dispersions: Saturn ring defects and quadrupolar interactions*, Eur. Phys. J. B 12 (1999), pp. 167–170.

[31] Y. Gu and N.L. Abbott, *Observation of Saturn-ring defects around solid microspheres in nematic liquid crystals*, Phys. Rev. Lett. 85 (2000), pp. 4719–4722.

[32] (a) R.W. Ruhwandl and E.M. Terentjev, *Long-range forces and aggregation of colloid particles in a nematic liquid crystal*, Phys. Rev. E 55 (1997), pp. 2958–2961; (b) R.W. Ruhwandl and E.M. Terentjev, *Monte Carlo simulation of topological defects in the nematic liquid crystal matrix around a spherical colloid particle*, Phys. Rev. E 56 (1997), pp. 5561–5565.

[33] T.C. Lubensky, D. Pettey, N. Currier, and H. Stark, *Topological defects and interactions in nematic emulsions*, Phys. Rev. E 57 (1998), pp. 610–625.

[34] H. Stark, *Director field configurations around a spherical particle in a nematic liquid crystal*, Eur. Phys. J. B 10 (1999), pp. 311–321.

[35] J. Fukuda, M. Yoneya, and H. Yokoyama, *Nematic liquid crystal around a spherical particle: investigation of the defect structure and its stability using adaptive mesh refinement*, Eur. Phys. J. E 13 (2004), pp. 87–98.

[36] M.S. Al-Barwani, G.S. Sutcliffe, and M.P. Allen, *Forces between two colloidal particles in a nematic solvent*, J. Phys. Chem. B 108 (2004), pp. 6663–6666.

[37] (a) G. de Luca and A.D. Rey, *Ringlike cores of cylindrically confined nematic point defects*, J. Chem. Phys. 127 (2007), 094907; (b) G. de Luca and A.D. Rey, *Point and ring defects in nematics under capillary confinement*, J. Chem. Phys. 127 (2007), 104902.

[38] G. Skačej and C. Zannoni, *Controlling surface defect valence in colloids*, Phys. Rev. Lett. 100 (2008), 197802.

[39] C. Völtz, Y. Maeda, Y. Tabe, and H. Yokoyama, *Director-configurational transitions around microbubbles of hydrostatically regulated size in liquid crystals*, Phys. Rev. Lett. 97 (2006), 227801.

[40] J.C. Loudet and P. Poulin, *Application of an electric field to colloidal particles suspended in a liquid-crystal solvent*, Phys. Rev. Lett. 87 (2001), 165503.

[41] S. Grollau, N.L. Abbott, and J.J. de Pablo, *Spherical particle immersed in a nematic liquid crystal: effects of confinement on the director field configurations*, Phys. Rev. E 67 (2003), 011702.

[42] (a) J. Fukuda, H. Stark, M. Yoneya, and H. Yokoyama, *Interaction between two spherical particles in a nematic liquid crystal*, Phys. Rev. E 69 (2004), 041706; (b) J. Fukuda and H. Yokoyama, *Separation-independent attractive force between like particles mediated by nematic- liquid-crystal distortions*, Phys. Rev. Lett. 94 (2005), 148301.

[43] (a) D.L. Cheung and M.P. Allen, *Structure of a liquid crystalline fluid around a macroparticle: density functional theory*, Phys. Rev. E 74 (2006), 021701; (b) D.L. Cheung and M.P. Allen, *Forces between cylindrical nanoparticles in a liquid crystal*, Langmuir 24 (2008), pp. 1411–1417; (c) D.L. Cheung and M.P. Allen, *Effect of substrate geometry on liquid-crystal-mediated nanocylinder-substrate interactions*, J. Chem. Phys. 129 (2008), 114706.

[44] (a) R. Yamamoto, *Simulating particle dispersions in nematic liquid-crystal solvents*, Phys. Rev. Lett. 87 (2001), 075502; (b) R. Yamamoto, Y. Nakayama, and K. Kim, *A smooth interface method for simulating liquid crystal colloid dispersions*, J. Phys.: Condens. Matter 16 (2004), pp. S1945–S1955.

[45] T. Araki and H. Tanaka, *Colloidal aggregation in a nematic liquid crystal: topological arrest of particles by a single-stroke disclination line*, Phys. Rev. Lett. 97 (2006), 127801.

[46] N. Sulaiman, D. Marenduzzo, and J.M. Yeomans, *Lattice Boltzmann algorithm to simulate isotropic-nematic emulsions*, Phys. Rev. E 74 (2006), 041708.

[47] C. Zhou, P. Yue, and J.J. Feng, *Dynamic simulation of droplet interaction and self-assembly in a nematic liquid crystal*, Langmuir 24 (2008), pp. 3099–3110.

[48] F.R. Hung, *Quadrupolar particles in a nematic liquid crystal: effects of particle size and shape*, Phys. Rev. E 79 (2009), 021705.

[49] (a) S.C. Glotzer, *Some assembly required*, Science 306 (2004), pp. 419–420; (b) S.C. Glotzer and M.J. Solomon, *Anisotropy of building blocks and their assembly into complex structures*, Nat. Mater. 6 (2007), pp. 557–562.

[50] (a) C.J. Murphy, T.K. Sau, A.M. Gole, C.J. Orendorff, J. Gao, L. Gou, S.E. Hunyadi, and T. Li, *Anisotropic metal nanoparticles: synthesis, assembly, and optical applications*, J. Phys. Chem. B 109 (2005), pp. 13857–13870; (b) J.A. Champion, Y.K. Katare, and S. Mitragotri, *Making polymeric micro- and nanoparticles of complex shapes*, Proc. Natl Acad. Sci. USA 104 (2007), pp. 11901–11904.

[51] Y. Sun and Y. Xia, *Shape-controlled synthesis of gold and silver nanoparticles*, Science 298 (2002), pp. 2176–2179.

[52] K.-S. Cho, D.V. Talapin, W. Gaschler, and C.B. Murray, *Designing PbSe nanowires and nanorings through oriented attachment of nanoparticles*, J. Am. Chem. Soc. 127 (2005), pp. 7140–7147.

[53] D. Dendukuri, D.C. Pregibon, J. Collins, T.A. Hatton, and P.S. Doyle, *Continuous-flow lithography for high-throughput microparticle synthesis*, Nat. Mater. 5 (2006), pp. 365–369.

[54] N. Malikova, I. Pastoriza-Santos, M. Schierhorn, N.A. Kotov, and L.M. Liz-Marzan, *Layer-by-layer assembled mixed spherical and planar gold nanoparticles: control of interparticle interactions*, Langmuir 18 (2002), pp. 3694–3697.

[55] O.D. Velev, *Self-assembly of unusual nanoparticle crystals*, Science 312 (2006), pp. 376–377.

[56] V.K. Gupta and N.L. Abbott, *Design of surfaces for patterned alignment of liquid crystals on planar and curved*, Science 276 (1997), pp. 1533–1536.

[57] A.N. Beris and B.J. Edwards, *Thermodynamics of Flowing Systems with Internal Microstructure*, Oxford University Press, New York, 1994.

[58] B.J. Edwards and A.N. Beris, *Order parameter representation of spatial inhomogeneities of polymeric liquid crystals*, J. Rheol. 33 (1989), pp. 1189–1193.

[59] B.J. Edwards, A.N. Beris, and M. Grmela, *Generalized constitutive equation for polymeric liquid crystals Part 1. Model formulation using the Hamiltonian (poisson bracket) formulation*, J. Non-Newton Fluid 35 (1990), pp. 51–72.

[60] N. Schopohl and T.J. Sluckin, *Defect core structure in nematic liquid crystal*, Phys. Rev. Lett. 59 (1987), pp. 2582–2584.

[61] COMSOL Multiphysics™ Version 3.4 User's Guide, COMSOL, Inc., Burlington, MA, 2007, and references therein. Available at http://www.comsol.com/.

[62] For the case of Equation (6), the elastic term $L_1\partial_k\partial_k Q_{ij}$ and the Landau–de Gennes terms were included as part of the diffusive flux (*c*) and source (*f*) terms, respectively, of the coefficient PDE form of COMSOL Multiphysics™. The models were created, executed and saved as a MATLAB® M-file.

[63] J. Fukuda, M. Yoneya, and H. Yokoyama, *Nematic liquid crystal around a spherical particle: investigation of the defect structure and its stability using adaptive mesh refinement*, Eur. Phys. J. E 13 (2004), pp. 87–98.

[64] (a) S. Kralj, E.G. Virga, and S. Žumer, *Biaxial torus around nematic point defects*, Phys. Rev. E 60 (1999), pp. 1858–1866; (b) S. Kralj and E.G. Virga, *Universal fine structure of nematic hedgehogs*, J. Phys. A: Math. Gen. 34 (2001), pp. 829–838; (c) S. Kralj and E.G. Virga, *Core hysteresis in nematic defects*, Phys. Rev. E 67 (2002), 021703.

[65] (a) A.C. Callan-Jones, A.R. Pelcovits, V.A. Slavin, S. Zhang, D.H. Laidlaw, and G.B. Loriot, *Simulation and visualization of topological defects in nematic liquid crystals*, Phys. Rev. E 74 (2006), 061701.

[66] G. McKay and E.G. Virga, *Mechanical actions on nanocylinders in nematic liquid crystals*, Phys. Rev. E 71 (2005), 041702.